Journal of Hazardous Materials, 14 (1987) 321–336
Elsevier Science Publishers B.V., Amsterdam — Printed in The Netherlands

SHOCK PROPAGATION AND BLAST ATTENUATION THROUGH AQUEOUS FOAMS*

TIMOTHY D. PANCZAK, HERMAN KRIER

Department of Mechanical and Industrial Engineering, University of Illinois, Urbana, IL 61801 (U.S.A.)

and P. BARRY BUTLER

Department of Mechanical Engineering, University of Iowa, Iowa City, IA 52242 (U.S.A.)

(Received November 5, 1985; accepted in revised form August 22, 1986)

Summary

Experiments cited in this paper reveal that aqueous foams are good attenuators of blast waves and the resulting noise. A model is presented which describes the behavior of an explosively produced blast wave propagating through aqueous foam. The equation of state for an air/water mixture is developed with specific attention to details of liquid water compressibility. Solutions of the conservation equations in a spherically one-dimensional form were performed using a finite-difference wave propagation code. Results are presented that indicate the effect of the foam expansion ratio as well as the dimensionless foam depth on the blast attenuation. The (limited) comparison of decibel level attenuation between the model and the experiments shows good agreement.

Introduction

Spherically symmetric blast waves resulting from explosions in air can cause serious damage to structures located many charge radii from the center. In addition, the blasts also produce significant levels of environmental noise at distances beyond the region of structural damage. Consequently, the areas where blast-producing activities (such as demolition work and ordnance disposal) can be conducted safely are limited.

When a detonation wave propagating through a condensed explosive reaches the air/explosive interface, an intense shock wave with pressures of the order of hundreds of atmospheres is propagated radially outward through the air. It has been shown [1] that the strength of the blast wave can be greatly attenuated by surrounding the explosive charge with aqueous foam. An aqueous

*Work supported by U.S. Army, Construction Engineering Research Laboratory, Champaign, IL; Dr. Richard Raspet was Program Monitor.

0304-3894/87/$03.50

foam consists of a matrix of thin sheets of water encapsulating tiny pockets of air. By adding a surfactant to the water to increase the surface tension, foam can be produced in a wide variety of expansion ratios. These foams are most commonly produced by commercial fire-fighting equipment. The expansion ratio is defined as the ratio of foam volume to liquid volume

$$\alpha = v_f/v_l \tag{1}$$

Raspet and Griffiths [1] summarize past experimental work on shock attenuation and include extensive data on far field attenuation of peak pressure, flat weighted integrated sound exposure levels (FSEL) and C-weighted exposure levels (CSEL) for a variety of charge masses, foam depths and foam expansion ratios. Also presented are scaling laws which relate the foam depth, foam density and charge mass to the noise reduction levels.

Figures 1a–c show reduction levels for various depths of 30:1 expansion ratio foam [1]. In these figures the foam depth is scaled to the cube root of the charge mass. The experiments were conducted using three different charge masses, 0.11 kg, 0.57 kg and 2.27 kg. The reductions are plotted in dBs (decibels) with the peak pressure level defined as 20 log (P_{max}/P_o) where P_{max} is the maximum pressure and P_o is a reference pressure, $P_o = 20\ \mu$Pa. The sound exposure level (SEL) is defined as

$$\text{SEL} = 10 \log \frac{\int P^2 dt}{P_o^{\,2}\, t_o} \tag{2}$$

where t_o is a reference time defined to be one second. The integral in eqn. (2) is performed over the entire duration of the wave form, both positive and negative phase. The FSEL is calculated with no frequency weighting and the CSEL is calculated with a standard C-weighting filter. In all configurations, two trials were performed and FSEL, CSEL and peak pressure were measured at both 60 m and 120 m from the charge center. Figures 2a–c show the 30:1 data combined with data for a much less dense 250:1 foam. Here, the authors included foam density ρ_f in the scaled depth. In Figs. 2a–c the dimensionless foam depth is defined as

$$X = \Delta r [\rho_f/M]^{1/3} \tag{3}$$

where ρ_f is the foam density [kg/m^3], Δr is the geometrically averaged foam depth [m], and M is the mass of the explosive [kg] (TNT equivalent).

In addition to peak pressure and sound exposure level reduction, Ref. [1] also notes a decrease in both the total and positive phase durations of the far field recorded wave form when foam is the wave propagation medium. Plotted as a function of scaled foam depth these dB reductions were 20% and 5%, respectively. As shown in Fig. 1, the maximum reductions in CSEL, FSEL and peak pressure were limited to about 10 dB.

An interesting result presented in Ref. [1] is that the attenuation is shown

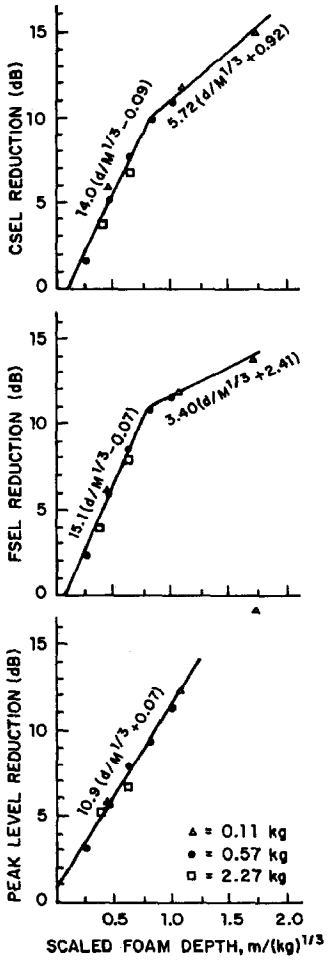

Fig. 1. Reductions for $\alpha = 30$ foam (from Ref. [1]). The scaled foam depth is defined as the ratio of foam depth d to the cube root of charge mass M.

to be linear with scaled foam depth up to a certain nondimensional depth (0.8 for 30:1, 1.5 for 250:1). For depths greater than this the foam still shows increasing attenuation with depth but at a much less effective rate. A two-mechanism model was proposed [1] to explain this bilinear behavior. First, it was assumed that in the near-field the shock pressure is strong enough to break the foam structure into microdroplets across the compressive shear layer of the shock front. This insures an extremely quick equilibration of velocity and temperature betweeen the two phases and allows one to consider the air/water foam system as a homogeneous material. Second, when the shock is no longer strong enough to shatter the foam structure, it is assumed that the air and

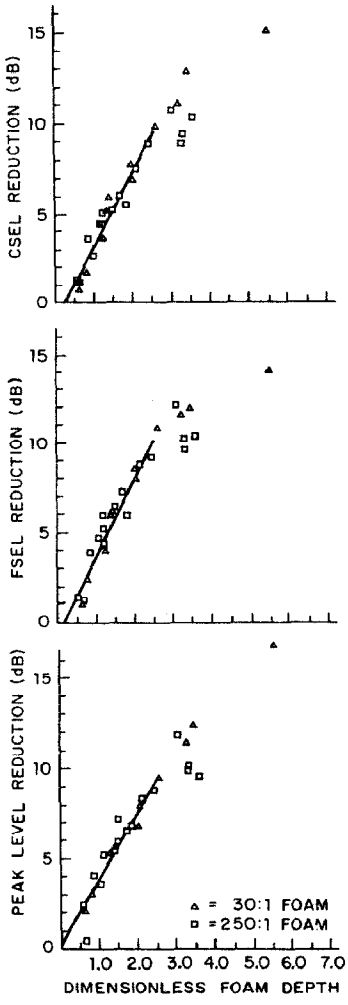

Fig. 2. Reductions versus dimensionless foam depth for $\alpha = 30$ and $\alpha = 250$ foam (from Ref. [1]). Dimensionless foam depth is defined in eqn. (3) of the text.

water components do not achieve immediate equilibrium. This lessens the degree of attenuation.

Much work has been done to explain the effectiveness of foam as a shock attenuator [2–4]. These works include theories based on multiple reflections from bubble surfaces and broadening of the shock due to bubble resonances. It should be noted that these mechanisms only occur in the acoustic or near acoustic range of overpressure and are probably not applicable to the extremely large overpressures encountered in explosively initiated shock waves. It was pointed out by Raspet and Griffiths [1] that the minimum shock strength needed to shatter the foam structure is on the order of several hundred kPa.

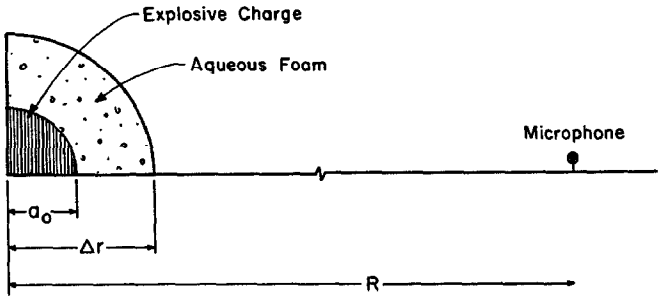

Fig. 3. Schematic of explosive/foam configuration.

Other experiments [5,6] have cited the vaporization of the water and the quenching of the afterburn as mechanisms which reduce the delayed energy imparted to the wave. We believe that the energy contribution by afterburn is a small percentage of the energy delivered by the initial detonation wave and is probably not the main mechanism for attenuation. The effects of vaporization will be examined in more detail later in this study.

The work presented here is by no means a detailed study of the pore surface structure within the foam. Instead, emphasis is placed on the hydrodynamic wave interactions within the medium and between material interfaces. Based on the strength of the explosively driven shock wave through the foam, the hydrodynamic model appears to be a valid approach. The following sections will outline the problem analysis, numerical solution technique and some results.

Analysis

Figure 3 defines the problem at hand. Located at the $r=0$ origin is a spherical charge of explosive with radius a_0. Surrounding the explosive is a foam with expansion ratio α and depth Δr. Surrounding the foam is air. For this analysis, the initial time is taken as the instant the detonation wave reaches the explosive/foam interface ($r=a_0$). The form of the detonation wave at this time is assumed to be the classical form of Taylor [7] for a spherical self-similar detonation wave profile. The magnitude of the transmitted and reflected waves at the foam boundary are calculated from the Rankine-Hugoniot jump conditions and the equations of state for the two materials (explosive, foam). In order to study the wave motion beyond this initial time, one must solve the equations of motion, equations of state, and the appropriate boundary and initial conditions for the entire flow field. For a one-dimensional, spherically symmetric analysis the equations of motion in Eulerian form are written as

Conservation of mass

$$\frac{\partial \rho}{\partial t} + u\frac{\partial \rho}{\partial r} + \rho\frac{\partial u}{\partial r} + 2\frac{\rho u}{r} = 0 \tag{4}$$

Conservation of momentum

$$\frac{\partial u}{\partial t} + u\frac{\partial u}{\partial r} + \frac{1}{\rho}\frac{\partial P}{\partial r} = 0 \tag{5}$$

Conservation of energy

$$\frac{\partial E}{\partial t} + u\frac{\partial E}{\partial r} - \frac{P}{\rho^2}\left(\frac{\partial \rho}{\partial r} + u\frac{\partial \rho}{\partial t}\right) = 0 \tag{6}$$

Equation of state

$$E = E(P, \rho) \tag{7}$$

At $r=0$ a reflected boundary condition is imposed and at $r=R$ a transmitted boundary condition is used. Internal boundary conditions at the material interfaces require continuity of particle velocity, u and pressure.

Along with appropriate initial conditions, the three nonlinear partial differential equations and the equation of state form a set of four equations to be solved for the four unknown variables E, P, u, and ρ. In order to obtain an analytical solution to this set of equations, some very limiting assumptions must be made [8–13]. A review of much of this work can be found in Ref. [14].

The solution technique used in the work performed here is based upon the finite difference solution to the governing differential equations and constitutive relations. A brief discussion of the solution technique follows.

Finite difference solution

The finite difference code used to solve the blast attenuation processes is an adaptation of the one-dimensional WONDY V code developed at Sandia Laboratories [15]. A detailed description of the operation of the code can be found in Ref. [15]. A brief discussion of the computational scheme, stability and ideal form of the state equation will be presented here.

The finite difference code is used to solve the set of one-dimensional equations of motion in spherical geometry. The governing equations written in Lagrangian form are

Conservation of mass

$$m = m_o \tag{8}$$

Conservation of momentum

$$\rho a = -\frac{\partial P}{\partial x} - \frac{\partial q}{\partial x} \tag{9}$$

Conservation of energy

$$\rho \frac{\partial E}{\partial t} = (P+q)\frac{1}{\rho}\frac{\partial \rho}{\partial t} \tag{10}$$

Equation of state

$$P = P(E, \rho) \tag{11}$$

Here, m represents the mass, ρ is the density, q is a viscous stress, P is the pressure, and E is the specific internal energy.

In the finite difference approximation to the differential equations all quantities sampled are material particles at discrete times. The differential equations are written in difference form by the use of centered, second-order analogs over a staggered computational grid. The space variables, a, u, and x (acceleration, velocity, and spatial location) are located at the cell boundaries, and the thermodynamic variables, P, E and ρ are centered in each cell.

Since the grid resolution of the code cannot be made small enough to accurately resolve the shock waves thickness, an apparent viscous stress q is introduced. This prevents the wave form from overtaking itself and increases computational stability by spreading the discontinuity across several cells. Shock waves in the finite difference solution are recognized as very steep but finite gradients in the solution. The form of q used in this work is

$$q = C_1 C_s \frac{\partial \rho}{\partial t} + C_2 \rho \left(\frac{1}{\rho}\frac{\partial \rho}{\partial t}\right)^2 \qquad \text{if } \frac{\partial \rho}{\partial t} > 0 \tag{12a}$$

$$q = 0 \qquad \text{if } \frac{\partial \rho}{\partial t} < 0 \tag{12b}$$

Here, C_1 and C_2 are constants [15] and C_s is the local sound velocity. In addition to providing numerical stability, the apparent viscous stress also satisfies the entropy production across the shock front as dictated by the second law of thermodynamics.

Equation of state for aqueous foam

When a shock passes through a liquid–gas mixture, the liquid requires a finite time to equilibrate velocity and temperature with the gas. In the relaxation zone, differences in velocity and temperature between the phases cause momentum and heat transfer which can have important effects on the resulting two-phase flow field. Often these processes proceed very rapidly, particu-

larly when one phase is finely dispersed in the other. When this happens it can be assumed that equilibrium is reached at the shock front and that the two component systems can be considered as a homogeneous pseudofluid that obeys the usual equations of single component flow.

As stated earlier, aqueous foam consists of a matrix of thin sheets of water encapsulating small pockets of air. In this analysis it is assumed that when a strong shock hits these thin sheets they are shattered into microdroplets by the viscous stress across the shock plane. This assumption is elaborated in Ref. [1]. Because of the droplets' size, they equilibrate very rapidly with the flowing gas. This assumption enables one to consider the system as an homogeneous entity, and thus use mass averaged thermodynamic properties to describe the system. These properties are weighted averages and are not necessarily the same as the properties of either phase. Pore surface structure is not treated in this work because of the strong shock overpressures.

In order to analyze shock propagation through foam using a finite difference method, one must first develop an equation of state for the homogeneous pseudofluid using average properties of the air and water components. The equation is then put in a form most amenable to hydrocode calculation, namely eqn. (11).

The task here is to find the fluid pressure given the fluid density and fluid internal energy using both the ideal gas equation of state with a nonconstant specific heat for air and an equation of state for water of the form $[P, E] = f\ (T, v)$. The water equation of state was supplied by Sandia Laboratories [15] and was found to be consistent to the fifth significant digit when compared with tabulated values from steam tables by Keenan, Keyes, Hill and Moore [16].

The equilibrium solution is found by satisfying the mixture mass (volume) and energy relations

mixture energy $$E_f = xE_a + (1-x)E_w \tag{13a}$$

mixture mass $$v_f = xv_a + (1-x)v_w \tag{13b}$$

where x = mass fraction of air, E = specific internal energy, and v = specific volume.

The subscripts f, a and w stand for fluid mixtures, air and water, respectively. In addition, we have the functional relations

$$E_a = f(T) = E_a(T) \tag{14a}$$

$$E_w = f(T, v_w) = E_w(T, v_w) \tag{14b}$$

$$v_a = RT/P_a \tag{14c}$$

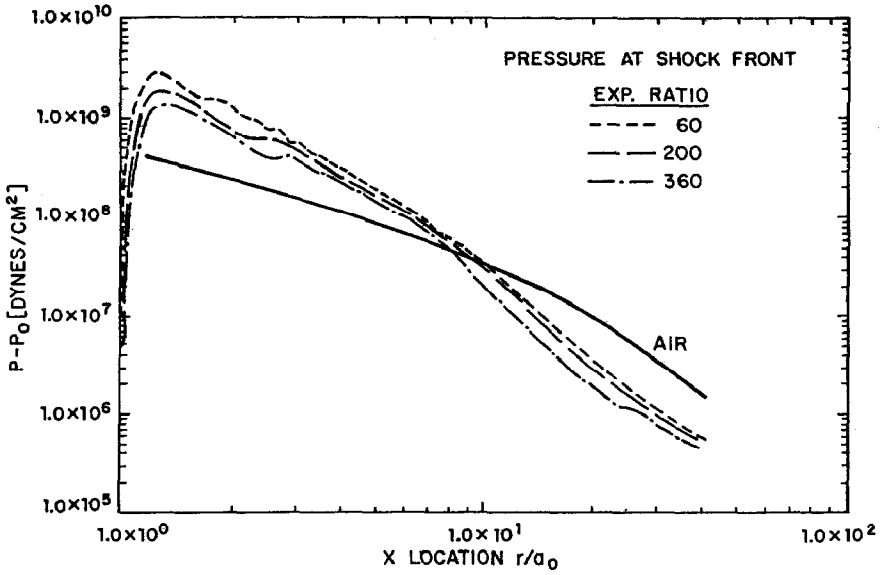

Fig. 4. Shock overpressure for various expansion ratio foams. For all cases, $\Delta r/a_0 = 40$.

$$P_w = f(T, v_w) = P_w(T, v_w) \tag{14d}$$

Assuming that the pressure and temperature of both phases are equal, we can rewrite the mass and energy relations as

$$E_f = xE_a(T) + (1-x)E_w(T, v_w) \tag{15a}$$

$$v_f = x\frac{RT}{P_w(T, v_w)} + (1-x)v_w \tag{15b}$$

The two equations are coupled through the fluid temperature, T, and the water specific volume, v_w. This provides two equations in two unknowns, T and v_w. The solution will yield the fluid pressure through the water equation of state, $P_w(T, v_w)$.

Since the internal energy of water is dependent on both temperature and specific volume (due to phase change) the temperature cannot be solved directly from the energy equation. If this were the case, pressure could be solved for by satisfying the mass relation, varying v_w. Since this is not possible, an iterative scheme must be employed to solve the two equations simultaneously.

Computed results

Figure 4 is a plot of the peak shock pressure as a function of distance from the charge center $r=0$. Three different expansion ratio foams (60,200,360)

are shown in the figure. Each case illustrated in Fig. 4 has a foam depth of $\Delta r/a_0 = 40$. Figure 4 also includes a plot of the locus of the peak shock pressure in an air medium (no foam $\alpha = \infty$) for the same charge [11]. The general trend is for the lower expansion ratio foams to start at a higher shock pressure than the air and higher expansion foams. The higher initial shock pressures for the lower expansion ratio foams is a result of the foam shock impedance and the product gas/foam interface boundary condition. Figure 4 also shows a break in the rate of pressure decrease at about 8 charge radii for the 60:1 foam; 9 charge radii for the 200:1 foam; and 10 charge radii for the 360:1 foam. The rate of pressure decay increases after this point. Evaluation of the thermodynamic properties shows that this break occurs when the lead shock is no longer of sufficient strength to vaporize the foam. This attenuation mechanism becomes evident when studying the pressure, energy and velocity histories of the attenuating flow fields.

Figures 5–7 show pressure, energy and density profiles for a constant expansion ratio (200:1) foam where the foam depth is 10 charge radii. In all six different depths were studied 5, 10, 15, 20, 30 and 40 charge radii, with the solutions integrated to a distance of 90 charge radii. Thermodynamic profiles for the remaining cases are not shown here, but can be found in Ref. [14]. These calculations were performed in order to investigate the blast wave behavior at the foam/air interface and to observe the effects of different foam depths on the far field wave form. The initial blast wave for these calculations was determined from an equation of state for TNT used by Brode [13] starting at the initial conditions specified by Taylor [7].

The results shown in Figs. 5–7 show the radial distance scaled to the initial charge radius. Pressure is scaled to ambient pressure (0.101 MPa) and density, energy and time are left unscaled. Also τ represents the elapsed time (μs) since the detonation wave reached the explosive/foam interface. It should be noted that prior to solving the flow equations with foam as the propagation medium, a test case was run for a standard charge in dry air. This particular test of the finite difference code was made since the corresponding experimental results are well documented [17]. The peak overpressures for this case were in favorable agreement with experimental observations in both the near-field and far-field.

Examining the results shown in Figs. 5–7, one can see that there is no significant difference in the pressure profiles other than that the second shock is attenuated more and is farther into the positive region as the depth increases. This does not explain the change in the rate of attenuation. However, inspection of the internal energy variations offers an explanation of the phenomena.

The increase in internal energy above the ambient is the last influence that the blast wave produces. The kinetic and thermal energy of the initial explosive products that goes into producing the blast wave will be distributed in the final state as an increase in the internal energy of the surrounding medium. When

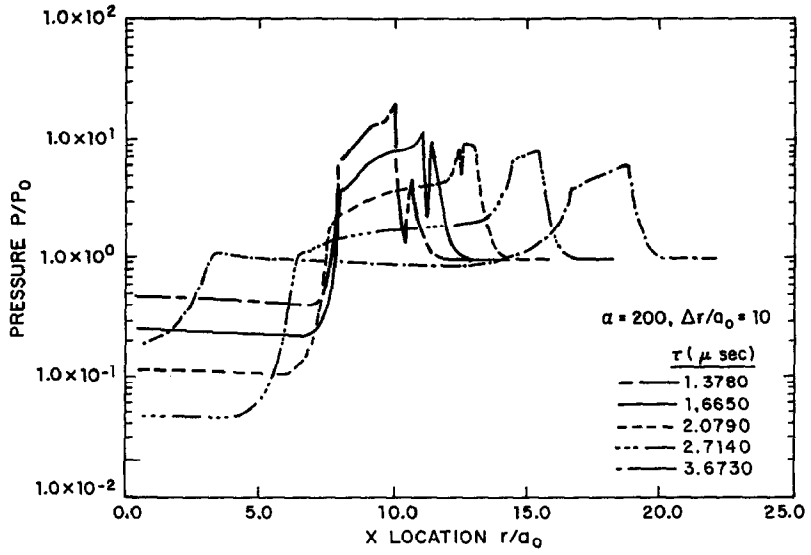

Fig. 5. Shock overpressure history for 200:1 expansion ratio foam, $\Delta r/a_0 = 10$.

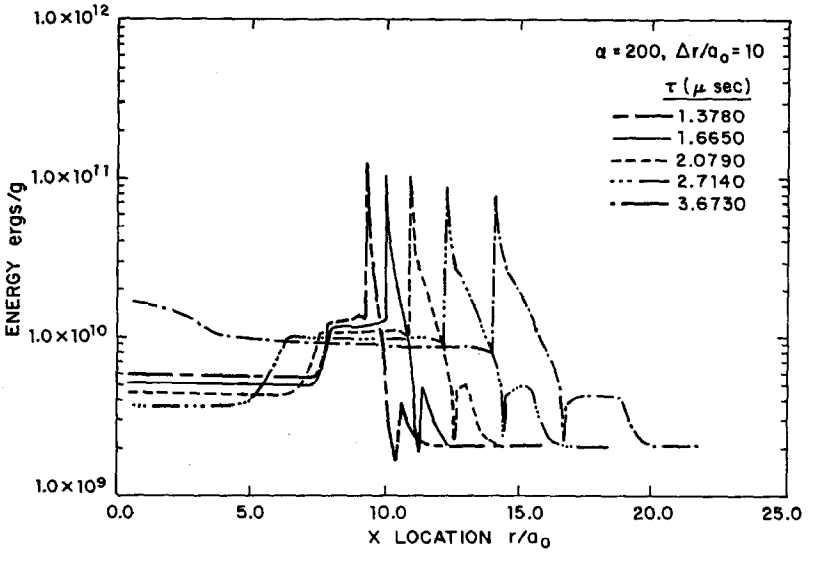

Fig. 6. Specific internal energy history for 200:1 expansion foam, $\Delta r/a_0 = 10$.

the shock wave passes a given location, it leaves the material at a pressure and energy determined by the jump conditions and the equation of state. When the medium expands back to ambient pressure, it returns some of this energy to the wave propagating ahead of it and retains some residual energy as a result of the irreversible heating caused by molecular shearing across the shock front. As the strength of the shock diminishes, the residual energy also diminishes.

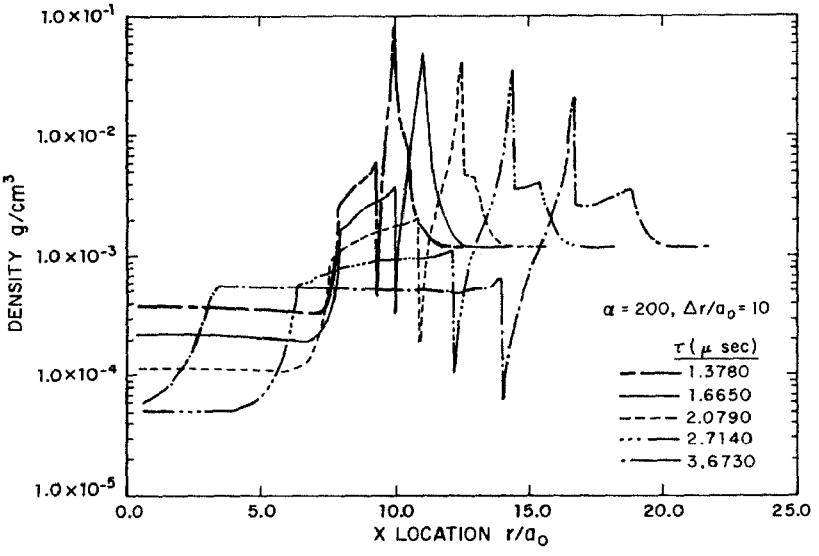

Fig. 7. Density history for 200:1 expansion ratio foam, $\Delta r/a_o = 10$.

In this weak shock case the wave can be thought of as propagating acoustically with the attenuation mostly due to spherical divergence. The spike in the internal energy–distance plots (Fig. 7) is due to the density discontinuity occurring at the material interface.

In order to make a comparison of the computed foam depth attenuation effectiveness with the data reported by Ref. [1], the data shown in Fig. 8 are presented as *reduction in dB* peak level in Fig. 9. Here, the dB reduction is relative to the overpressure predicted for an r/a_o of zero. Figure 8 shows this to be 185.8 dB. Thus, for example, a normalized foam depth of 10 would give a dB reduction of $185.8 - 183.2 = 2.6$. The predicted dB reductions for five different cases of r/a_o are shown in Fig. 9. Also shown (as a solid line) for comparison is the measured far-field peak level dB reduction for an $\alpha = 250$ foam, taken from Fig. 3 of Ref. [1].

A least-squares fit of the predicted Peak Level Reduction $(\mathrm{PLR})_{\mathrm{dB}}$ for normalized foam depths less than 25 is,

$$(\mathrm{PLR})_{\mathrm{dB}} = 0.28\ (\Delta r_{\mathrm{foam}}/a_o) - 0.04 \tag{16}$$

In order to compare this with the data presented in Ref. [1] (as shown in Fig. 9) it was necessary to first carry out some conversions, since the data (Fig. 3 of Ref. [1]) are presented as $(\mathrm{PLR})_{\mathrm{dB}}$ versus scaled foam depth $(r/M^{1/3})$. This depth is the ratio of foam depth divided by the cube root of the explosive charge mass. In terms of that parameter, the best-fit equation for the $\alpha = 250$ foam was a far-field dB reduction that is given by

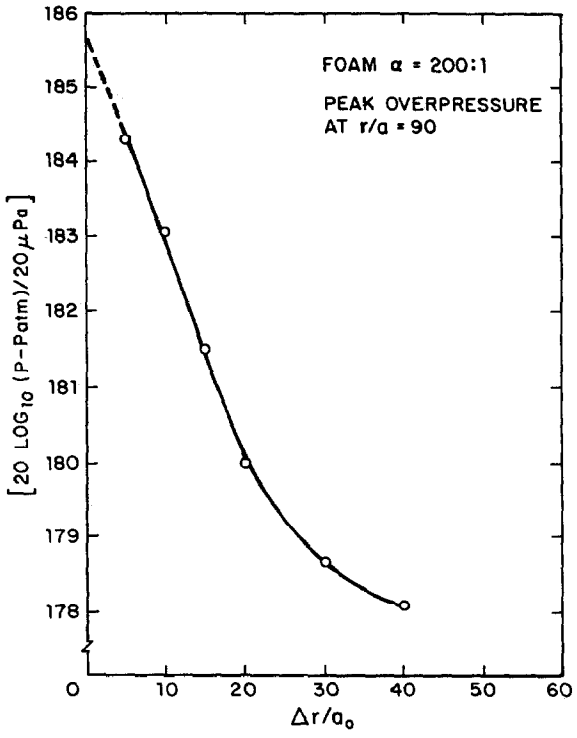

Fig. 8. Predicted "far-field" overpressure decibel level as a function of normalized foam thickness (α=200 foam).

$$(\mathrm{PLR})_{\mathrm{dB}} = 6.33\ (\Delta r_{\mathrm{f}}/M^{1/3} - 0.03) \qquad \text{for } 0 \leqslant \Delta r_{\mathrm{f}}/M^{1/3} \leqslant 1.5 \tag{17}$$

Since the explosive used in the experiments was C-4, not TNT, it was necessary to scale the mass of C-4 to an equivalent TNT mass of TNT, $M_{\mathrm{TNT}} = 1.35\ M_{\mathrm{C\text{-}4}}$. Therefore, to determine the equivalent charge radius, a_{o} (as used in the computer prediction)

$$M_{\mathrm{C\text{-}4}}{}^{1/3} = (M_{\mathrm{TNT}}/1.34)^{1/3} = 1.73\,(4\pi\rho_{\mathrm{TNT}}/3)^{1/3} a_{\mathrm{oTNT}} \tag{18}$$

Thus 1 kg of C-4 explosive is equivalent to a mass of TNT with $a_{\mathrm{oTNT}} = 0.04$ m.

When substituting this relation into eqn. (17) one obtains the experimental best least-squares fit, as

$$(\mathrm{PLR})_{\mathrm{dB}} = 0.366\ (\Delta r_{\mathrm{f}}/a_{\mathrm{o}}) - 0.19 \qquad \text{for } 0 \leqslant r/a_{\mathrm{o}} \leqslant 26 \tag{19}$$

This equation is shown by the solid line in Fig. 9 and compares favorably with eqn. (16).

Conclusions

The results presented show an increase in the rate of attenuation after the shock no longer vaporizes the water component of the mixture, leading one to

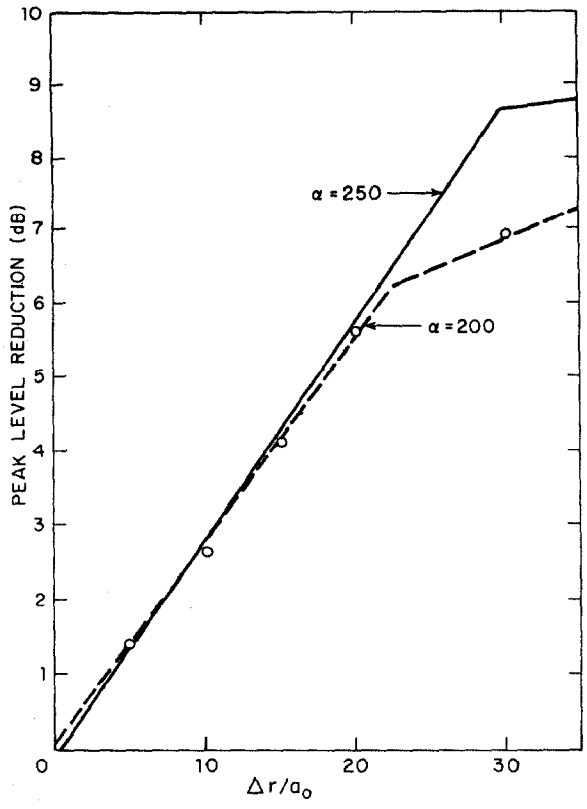

Fig. 9. Comparison of the predicted decibel peak level reduction (in the "far-field") with experiments from Ref. [1] (solid line).

conclude that vaporization can in fact be detrimental to maximum attenuation. When the liquid component of the system vaporizes, the air is no longer loaded with a relatively incompressible material and the shock speed increases. This enables secondary shocks to catch up to and reinforce the main shock. This aspect of phase change is also detrimental to attenuation in the intermediate field. The greater propagation speed of the secondary shocks may also account for the reduced duration of the negative phase.

The many wave reflections off the foam/air interface produce a complicated waveform in this region. However, it was noted that these disturbances rapidly decay into the air region and are small compared to the peak disturbance. For smaller foam depths the transmitted pressure is still high, and nonacoustic attenuation by the air adjacent to the foam occurs.

A significant pressure drop occurs at the foam/air interface for small foam depths, and in this respect, the impedence mismatch between the air and the foam is important. However, for large foam depths, where the attenuation due to shock dissipation occurs solely in this region, the effects of reflections from

the foam/air surface and the impedence mismatch have little influence on the far field waveform.

Two factors are responsible for determining the amount of residual heat left in the medium once the shock has passed. One is the thermodynamic properties that influence the conditions across the shock discontinuity. For maximum attenuation (for a given pressure) one would wish to maximize the rise in internal energy across the shock and minimize the drop in energy during isentropic expansion back to ambient pressure. This effect is determined solely by the equation of state of the medium. The other contributing factor is that, for the same material, a higher pressure shock produces a larger amount of residual energy. Thus, for large foam depths where interface interactions are minimal, the two most important factors contributing to high attenuation are a maximum initial overpressure and the ability to produce a high residual energy. In addition, the lower expansion ratio foams attenuate more than light foams for two possible reasons. The first is that the initial overpressure is higher and the second is that for a given pressure, more residual energy is produced. It is likely that both factors contribute.

Beyond a certain foam depth the amount of residual energy left in the region of expanded foam drops sharply. Most of the energy imparted to the foam by the shock is then returned to the wave upon expansion. Attenuation past this point is due mostly to divergence.

Acknowledgement

The authors acknowledge Dr. Stewart Griffiths, Sandia National Laboratories, Albuquerque, NM, for his input into the equation of state analysis.

References

1 R. Raspet and S.K. Griffiths, The reduction of blast noise with aqueous foam, J. Acoust. Soc. Amer., 74(6) (1983) 1757–1763.

2 D.L. Evans, D.F. Jankowski and E.D. Hirleman, A preliminary investigation of aqueous foam for blast wave attenuation, ERC-R-78050, College of Engineering and Applied Sciences, Arizona State University, Tempe, AZ, January 1979.

3 J.S. de Krasinski and A. Khosla, Shock attenuation in non-homogeneous and porous media, Report No. 34, University of Calgory, Canada, Department of Mechanical Engineering, March 1972.

4 V. Ramesh and J.S. de Krasinski, Shock and flame tube laboratory experiments, Report No. 73, University of Calgory, Canada, Department of Mechanical Engineering, March 1976.

5 A.K. Clark, P.J. Hubbard, P.R. Lee and H.C. Woodman, The reduction of noise levels from explosive test facilities using aqueous foams, NSWC/WO2 TR 77-36, NSWL, July 1977.

6 D.A. Dadley, E.Q. Robinson and V.C. Pickett, The use of foam to muffle blast from explosions, Paper presented at the IBP-ABCA Meeting, June 1976.

7 G.I. Taylor, The dynamics of the combustion products behind plane and spherical detonation fronts in explosives, Proc. R. Soc. London, Ser. A, 200 (1950) 235.

8 G.I. Taylor, The air wave surrounding an expanding sphere, Proc. R. Soc., London, Ser. A, 186 (1946) 273-292.
9 A.H. Taub (Ed.), John Von Neumann Collected Works, Vol. VI, Pergamon Press, New York, 1963.
10 L.I. Sedov, Similarity and Dimensional Methods in Mechanics, Academic Press, New York, 1959.
11 S. Griffiths, Aqueous foam blast attenuation, internal report, Sandia Laboratories, New Mexico; Private communication to Professor Herman Krier and Dr. Richard Raspet, September 1982.
12 S.R. Brinkley and J.G. Kirkwood, Theory of the propagation of shock waves, Phys. Rev. 71(9) (1947) 606-611.
13 H.L. Brode, Blast wave from a spherical charge, Phys. Fluids, 2(2) (1959).
14 T.D. Panczak and H. Krier, Shock propagation and blast attenuation through aqueous foams, UILU ENG 83-4007, University of Illinois, 1983.
15 M.E. Kipp and R.J. Lawrence, WONDY V — A one-dimensional finite-difference wave propagation code, SAND81-0939, Sandia Laboratories, NM, June 1982.
16 J.H. Keenan, F.G. Keyes, P.G. Hill and J.G. Moore, Steam Tables, John Wiley & Sons, New York, 1969.
17 W.E. Baker, Explosions in Air, University of Texas Press, Austin, 1973.